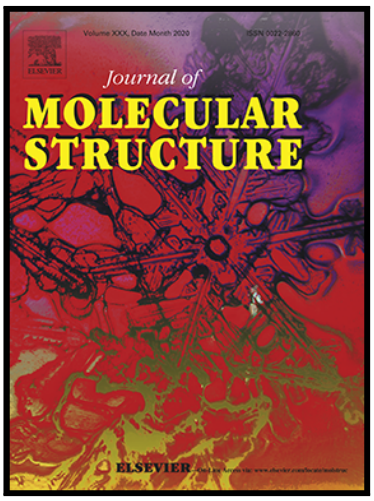

2-Benzyloxynaphthalene Aminoalkylated Chalcone Designed as Acetylcholinesterase Inhibitor: Structural Characterisation, in vitro Biological Activity and Molecular Docking Studies

Ghadah Aljohani , Adeeb Al-Sheikh Ali , Musa A. Said , David L. Hughes , Shaya Y. Alraqa , Syazwani Amran , Farediah Ahmad , Norazah Basar

PII: S0022-2860(20)31223-0
DOI: https://doi.org/10.1016/j.molstruc.2020.128898
Reference: MOLSTR 128898

To appear in: *Journal of Molecular Structure*

Received date: 27 April 2020
Revised date: 11 July 2020
Accepted date: 13 July 2020

Please cite this article as: Ghadah Aljohani , Adeeb Al-Sheikh Ali , Musa A. Said , David L. Hughes , Shaya Y. Alraqa , Syazwani Amran , Farediah Ahmad , Norazah Basar , 2-Benzyloxynaphthalene Aminoalkylated Chalcone Designed as Acetylcholinesterase Inhibitor: Structural Characterisation, in vitro Biological Activity and Molecular Docking Studies, *Journal of Molecular Structure* (2020), doi: https://doi.org/10.1016/j.molstruc.2020.128898

Highlights

- A novel chalcone was characterized using NMR, IR, UV-Vis, XRD and HSA analysis.
- The chelating studies with some metal chloride were performed using UV-vis.
- The chalcone shows biometal chelating ability and moderate antioxidant activity.
- The bio-studies of chalcone revealed 33-fold better inhibition than donepezil.
- A molecular modelling study of the chalcone shown dual binding inhibition of AChE.

2-Benzyloxynaphthalene Aminoalkylated Chalcone Designed as Acetylcholinesterase Inhibitor: Structural Characterisation, in vitro Biological Activity and Molecular Docking Studies

Ghadah Aljohani[a,b], Adeeb Al-Sheikh Ali[a], Musa A. Said [a]*, David L. Hughes[c], Shaya Y. Alraqa[a], Syazwani Amran[d], Farediah Ahmad[b], Norazah Basar[b*]

[a] Chemistry Department, Taibah University, P.O. Box 30002, Code 14177, Al-Madinah Al Munawarah, Kingdom of Saudi Arabia

[b] Department of Chemistry, Faculty of Science, Universiti Teknologi Malaysia, 81310 Johor Bahru, Johor, Malaysia

[c] School of Chemistry, University of East Anglia, Norwich, NR4 7TJ, United Kingdom,

[d] Department of Biosciences, Faculty of Science, Universiti Teknologi Malaysia, 81310 Johor Bahru, Johor, Malaysia

Abstract:

The design of an acetylcholinesterase inhibitor with multifunctional properties became the perspective for the development of an effective drug against Alzheimer's disease. Towards this target, 1-{4-hydroxy-3-[(piperidin-1-yl)methyl]phenyl}ethan-1-one (chalcone **3**) was prepared and studied as an acetylcholinesterase inhibitor. The novel chalcone **3** was synthesised via Claisen-Schmidt condensation reaction with 84% yield and characterized using 1D and 2D NMR spectroscopy. The *in vitro* bioactivity studies of chalcone **3** demonstrated excellent inhibitory activity against AChE (IC_{50} 1.0 nM) showing 33-fold better inhibition than donepezil, biometal chelating ability and moderate antioxidant activity. Chalcone **3** with these fascinating multifunctional proprieties can be a good candidate for the development of AD treatments. A molecular modelling investigation revealed that chalcone **3** showed dual binding inhibition of AChE enzyme. XRD shows short intra- and inter-molecular interactions with two chalcone **3** molecules per cell. Interesting Hirshfeld Surface Analysis (HSA) was conducted showing explicit agreement with the XRD analysis.

Keywords:

Acetylcholinesterase (AChE); metal chelation; NMR titration, molecular docking, XRD, Hirshfeld Surface Analysis

1. Introduction

Chalcones are α,β unsaturated carbonyl compounds with a 1,3-diphenyl-2-propene-1-one framework [1]. They are open-chain flavonoids with two aromatic rings linked by an aliphatic three-carbon chain. Chalcones are an essential component in natural products and play a key role in synthetic manipulations [2].

Although naphthalene has toxic effects [3], some of its derivatives are bestowed with medicinal value [4], and several of them have been characterised as antioxidants [5]. Considering both the cytotoxic and antioxidant properties of naphthalene derivatives, organic and medicinal chemists are trying to design drugs that have maximum therapeutic index and minimum toxicity so that they can be used as therapeutics [6]. Some investigations have been conducted to synthesise chalcones using naphthaldehyde [7,8].

Alzheimer's disease (AD) has received considerable attention because it is the most common cause of dementia. According to the World Health Organization, it accounts for 60–70 per cent of dementia cases worldwide [9]. Cholinesterase inhibitors (ChEIs) are the only class of agents that have so far consistently proved effective in treating the cognitive and functional symptoms of AD [10]. Medications approved by the U.S. Food and Drug Administration (FDA) for AD belong to a category of acetylcholinesterase inhibitors, but most of them were found to have side effects [11].

A trend has developed recently to use naturally occurring and synthetic derivatives of chalcones as cholinesterase inhibitors due to their slight side effects [12]. Recent studies on AD have confirmed that a Mannich base and chalcone, when incorporated into a single pharmacophore, displayed moderate inhibitory effect for AChE with excellent multifunctional properties [13,14].

Metal chelators and reactive oxygen species (ROS) scavengers have demonstrated potential therapeutic capacity in treating AD due to the increased level of metal ions in the plaque [15]. Iron, copper and zinc are essential elements for properly maintaining neurological functions in the brain. However, their abnormal levels have been observed in several subcortical regions of the AD brain tissues [16]. N-terminal amino acid residues contain metal binding sites that are capable of coordinating transition metal ions with high affinity. These metal ions significantly affect the aggregation behaviour of Amyloid β-protein (Aβ) [17,18]. Metal-binding at these sites can accelerate Aβ

aggregation and generate more amorphous aggregates, including neuro-toxic oligomers [19]. A relationship between increased aluminium exposure and AD has been found in some studies [20]. It has been also reported that aluminium can play a role in the aetiology of AD because of its ability to increase oxidative stress caused by iron and other metals [21].

This study is a follow-up of our comprehensive research on designing and synthesising chalcone derivatives as acetylcholinesterase inhibitors using Mannich bases. Hence, the spectroscopic data for 1-{4-hydroxy-3-[(piperidin-1-yl)methyl]phenyl}ethan-1-one (chalcone **3**) have been invesitgated to help understand the structural and geometrical features of the novel chalcone in the crystal lattice. To investigate possible binding interactions with the target enzyme, a molecular modelling study was performed using the experimental crystal structure data of the title compound **3**. Hirshfeld Surface Analysis (HSA) clarifies details of intermolecular interactions derived from the X-ray analysis.

2. Experimental

2.1 Synthesis of chalcone

2-Benzyloxy-1-naphthaldehyde **(1)** was obtained *via* an alkylation reaction of commercially available 2-hydroxy-1-naphthaldehyde in a typical, published procedure [22]. 1-{4-Hydroxy-3-[(piperidin-1-yl)methyl]phenyl}ethan-1-one **(2)** was synthesised by means of the Mannich reaction of 4-hydroxyacetophenone with piperidine and formaldehyde according to the method reported earlier [23]. The starting materials underwent a Claisen-Schmidt condensation reaction to produce chalcone **3** as yellow crystals in an excellent yield (84%) with melting point of 137-140 ℃ (**Scheme 1**) [24–26].

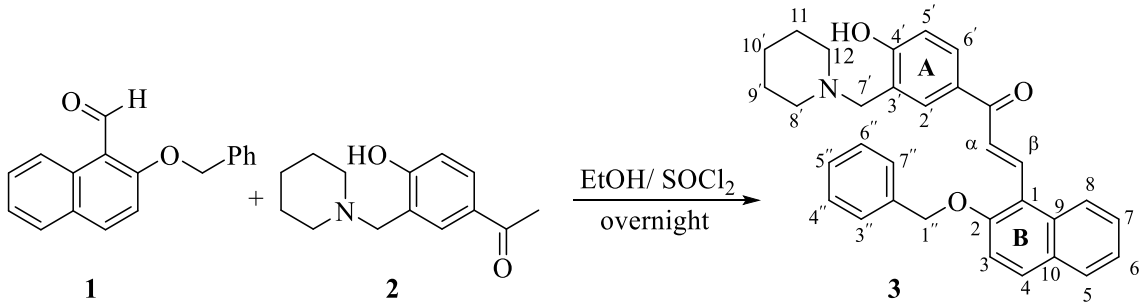

Scheme 1. Synthetic route to the title chalcone **3**.

*2.2 Crystal structure of chalcone **3** and Hirshfeld Surface Analysis*

Recrystallisation of chalcone **3** using cold ethanol provided a suitable crystal for X-ray analysis. Crystals are pale yellow plates and, from a sample under oil, one, *ca* 0.23 x 0.28 x 0.43 mm, was mounted on a glass fibre and fixed in the cold nitrogen stream on an Oxford Diffraction Xcalibur-3/Sapphire3-CCD diffractometer, equipped with Mo-Kα radiation and graphite monochromator. Intensity data were measured by thin-slice φ-scans. Total no. of reflections recorded, to θ_{max} = 27.5°, was 23161 of which 6372 were unique (Rint = 0.037); 4826 were observed with $I > 2\sigma_I$.

Data were processed using CrysAlis PRO 1.171.39.46 [27] for cell refinement and data reduction. Program used to solve structure: SHELXT [28a]; program used to refine structure: SHELXL2014/7 [28b]; molecular graphics: ORTEP [29]; software used to prepare material for publication: SHELXL2014/7 [28b] and WinGX [29].

Crystal data: $C_{32}H_{31}NO_3$, C_2H_6O, M = 523.64. Triclinic, space group P-1 (no. 2), a = 10.6946(5), b = 11.7088(5), c = 13.5975(5) Å, α = 96.356(4), β = 107.209(4), γ = 116.643(5) °, V = 1393.45(12) $Å^3$. Z = 2, Dc = 1.248 g cm^{-3}, F(000) = 560, T = 140(1) K, μ(Mo-Kα) = 0.81 cm^{-1}, λ(Mo-Kα) = 0.71073 Å.

Hirshfeld surface analysis and the related 2D-fingerprint plots were calculated using Crystal Explorer, which reads a structure input file in CIF format [30].

2.3 Metal-chelating studies

The metal chelating studies were performed on chalcone **3** using the Shimadzu UV-1601 spectrophotometer and Bruker 400MHz NMR spectrometer. The UV−Vis absorption spectra of chalcone **3** in methanol (50 μM) alone and in the presence of $CuCl_2$, $ZnCl_2$, $AlCl_3$, and $FeCl_2$ (50 μM in methanol) were recorded with wavelength ranging from 200 to 600 nm *in situ* at room temperature. The molar ratio method was used to determine the stoichiometry of the complex **3**-Fe^{2+} by titrating the methanol solution of chalcone **3** in a fixed concentration (60 μM) with increasing concentration of $FeCl_2$ (6-100 μM). The UV−Vis spectra were recorded at 307 nm and treated by numerical subtraction of $FeCl_2$ and **3** at corresponding concentrations, plotted *versus* the mole fraction of **3**. For NMR titrations, chalcone **3** (9 mg, 0.019 mmol) was dissolved in CD_3OD (1 mL) for ^{1}HNMR analysis using a micro NMR tube and the spectrum was recorded before titration. Then $FeCl_2$ (19 μM) solution (in D_2O) was titrated progressively using a micropipette within the NMR tube to monitor the ^{1}HNMR *in situ*. Spectra 2-6 were recorded upon the addition of the increasing equivalents of $FeCl_2$.

*2.4 In vitro bioactivity studies of chalcone **3***

2.4.1 Antionxidant activity analysis

The antioxidant evaluation was performed against 2,2-diphenyl-1-picrylhydrazyl (DPPH) free radical based on the method described by Hamad *et al.* [31]. A series of dilutions ranging from 10 μg/ml to 13 mg/ml was prepared in methanol. An aliquot of 40 μL of chalcone 3 from each serial dilution was mixed with 160 μL of freshly prepared methanolic solution of 100 μM DPPH radical and kept in the dark. After 30 min of incubation, the decrease in absorbance at 517 nm was determined. The absorbance of the DPPH radical without antioxidant (blank) and the reference compound ascorbic acid were also measured. All the determinations were performed in three replicates and averaged. The percentage inhibition of the DPPH radical was calculated according to the formula:

$$\text{Percentage Inhibition (\%)} = \frac{(A_{blank} - A_{sample})}{A_{blank}} \times 100$$

where A_{blank} = absorbance of the blank solution (containing DPPH solution without sample) and A_{sample} = absorbance of a sample solution. The concentration affording 50% inhibition (IC_{50}) values were calculated using GraphPad Prism for Windows (version 8.3.0) software.

2.4.2 Inhibition of AChE enzyme activity

The acetylcholinesterase inhibitory activity of chalcone **3** was determined by Ellman's microplate assay described by Koay *et al.*(2014) [32]. 140 µl of 0.1 M sodium phosphate buffer (pH 8) was added first followed by 20 µl of the test sample (in 10% methanol) and 20 µl of 0.09 unit/ml AChE from *Electrophorus electricus* (*Electric eel*). After pre-incubation at room temperature, 10 µl of 10 mM 5,5′-dithiobis (2-nitrobenzoic acid) DTNB was added into each well followed by 10 µl of 14 mM acetylthiocholine iodide as substrate. The absorbance of the coloured product was measured using a microplate reader at 412 nm following 30 minutes incubation. Donepezil hydrochloride (Sigma-Aldrich) was used as a positive control. Percentage inhibition was calculated using the following formula for eight different concentrations:

$$\text{Percentage Inhibition (\%)} = \frac{(\text{absorbance of control} - \text{absorbance of sample})}{\text{absorbance of control}} \times 100$$

Three replicates of the sample were used for statistical analysis with values reported as mean ± S.D. Standard curves were generated and the 50% inhibitory concentration (IC_{50}) values were calculated using GraphPad Prism.

2.5 Molecular docking

A docking study was carried out using AUTODOCK 4.2 [33]. The X-ray crystal structure of the acetylcholinesterase complexed with donepezil (PDB code: 1EVE) was obtained from the Protein Data Bank (https://www.rcsb.org/structure/1eve). All ligands and water molecules were removed from the retrieved protein using Discovery Studio Visualizer v17.2.0.16349 [34]. The experimental crystal structure of chalcone **3** was converted to PDB file and used for docking after the removal of the co-solvent (ethanol). The

chalcone-protein interactions were analysed and visualised in two-dimensional (2D) diagrams using Discovery Studio Visualizer.

3. Results and discussion

3.1 Spectral analysis

The ^{1}H NMR spectrum of chalcone **3** showed an AB spin system at δ_H 7.97 and 8.36 (d, *J* = 15.4 Hz) attributed to H-β and H-α, respectively as presented in **Fig. 1**. These two doublets are characteristic of the *trans*-olefinic protons of chalcone. The remaining aromatic protons were assigned based on the COSY spectrum **(Fig. 2)**. The ^{13}C NMR and DEPT spectra displayed twenty-eight carbon signals, including five methylenes, fourteen methines, eight quaternaries and one carbonyl carbon **(Fig. S1)**. The HMQC spectrum displayed direct correlations between protons and carbons in the compound, thus confirmed the assignment of the protonated carbon peaks at δ_C 22.78 (C-9′/11), 71.20 (C-1″), 128.67 (C-5″), 128.74 (C-4″/6″), 129.10 (C-3″/7″) **(Fig. S2)**. HMBC spectrum was reported to confirm the assignment of protons and carbons. The spectrum **Fig. S3** exhibited the presence of correlation between A_2B_2 aromatic protons at δ_H 7.57-7.63 (H-3", H-7") with C-4",6 " (δC 128.74), while protons at δ_H 7.38-7.47 (H-4″, H-6″) were correlated with C-3",7 " (δ_C 129.10) and C-5" (δ_C 128.67). The complete ^{1}H, ^{13}C, COSY, HMQC and HMBC spectral data of chalcone **3** are listed in **Table 1**.

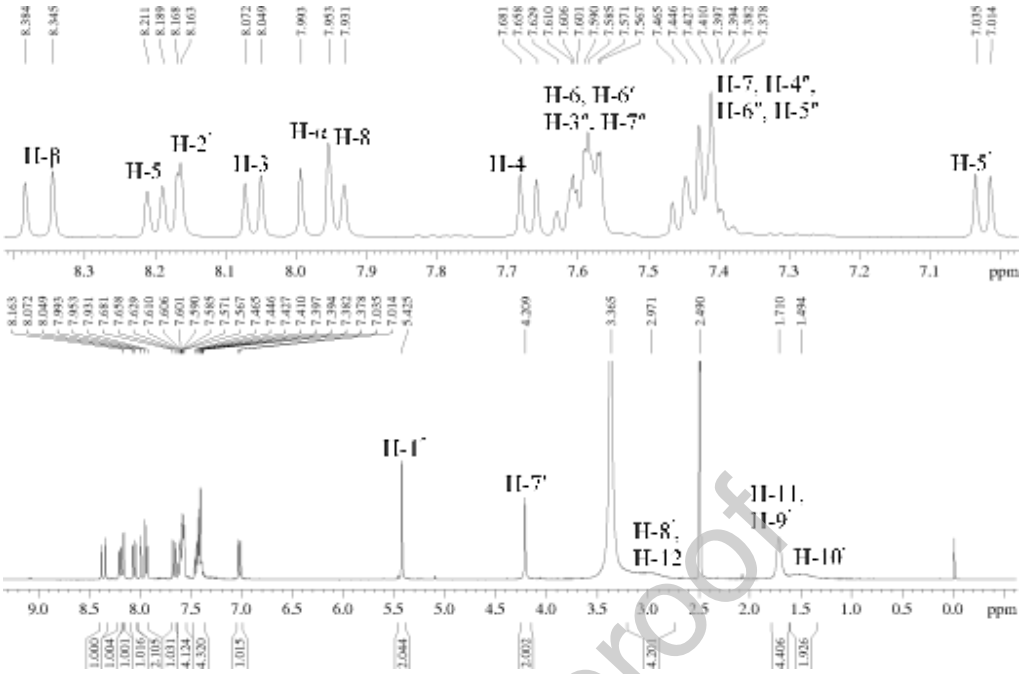

Fig. 1 ^{1}H NMR spectrum of chalcone **3**

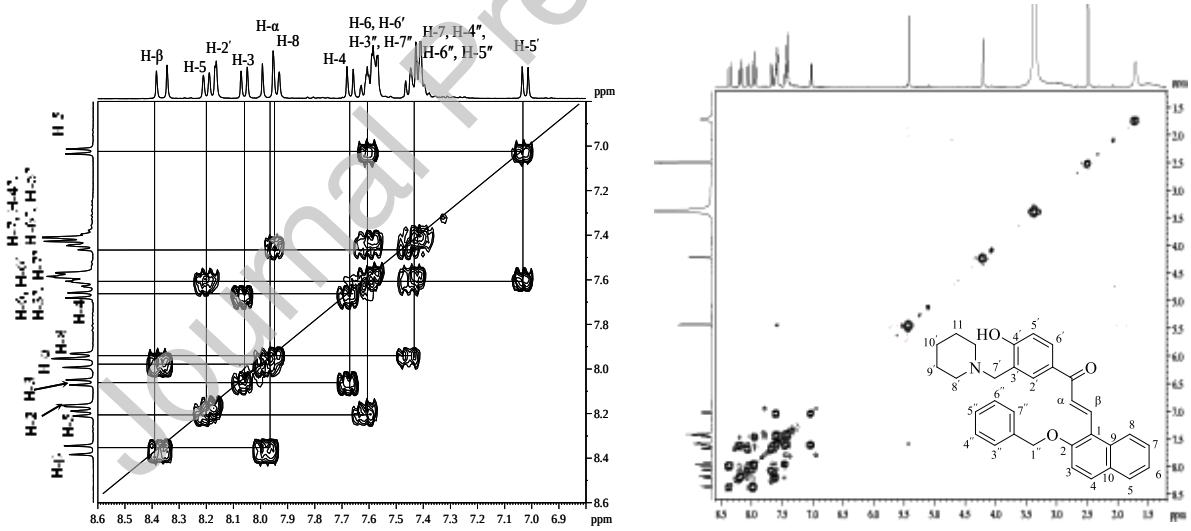

Fig. 2 ^{1}H-^{1}H COSY spectrum of chalcone **3**

Table 1 NMR Spectroscopic data of chalcone **3**

Position	δ_H	δ_C	COSY	HMBC

1	-	132.93		
2	-	156.84		
3	8.06 (d, *J* = 9.2 Hz)	132.54	H-4	C-2, C-1
4	7.67 (d, *J* = 9.2 Hz)	115.15	H-3	C-2, C-9, C-10
5	8.20 (d, *J* = 8.8 Hz)	123.19	H-6	C-7, C-9, C-10
6	7.57-7.63 (m)	128.36	H-5, H-7	C-8
7	7.38-7.47 (m)	124.53	H-6, H-8	C-5
8	7.94 (d, *J* = 8.8 Hz)	129.30	H-7	C-1, C-6, C-10
9	-	129.18		
10	-	116.77		
α	7.97 (d, *J* = 15.8 Hz)	126.76	H- β	C=O, C-1
β	8.36 (d, *J* = 15.8 Hz)	136.06	H- α	C=O, C-2, C-1, C-α
1′	-	129.74		
2′	8.16 (d, *J* = 2.0 Hz)	134.91		C-4′, C-6′, C-7′
3′	-	117.17		
4′	-	161.76		
5′	7.02 (d, *J* = 8.8 Hz)	116.06	H-6′	C-1′, C-3′, C4′
6′	7.57-7.63 (m)	132.16	H-5′	C-4′, C-2′
7′	4.21 (s)	54.02		C-2′, C-3′, C4′, C-8′
8′, 12	2.97 (br s)	52.32		
9′, 11	1.75 (br s)	22.78		
10′	1.50 (br s)	21.66		
1″	5.43 (s)	71.20	H-3″, H-7″	C-2, C-2″, C-3″, C-7″
2″	-	137.17		
3″, 7″	7.57-7.63 (m)	129.10		C-4″, C-6″
4″, 6″	7.38-7.47 (m)	128.74		C-3″, C- 7″, C-5″
5″	7.38-7.47 (m)	128.67		
C=O	-	187.88		

Experimental data measured at 400 MHz in DMSO

*3.2 Crystal structure analysis of chalcone **3** and Hirshfeld Surface Analysis*

Details of data collection, parameters, crystallographic data and final agreement parameters are collected in **Table 2**. Selected bond angles and distances are collected in **Table 3**. The molecular structure of **3** with atomic numbering is shown in **Fig. 3(a)** and **Table 4**. With one co-crystallized solvent molecule, X-ray single-crystal structural analysis revealed that compound **3** is triclinic, space group P-1, with two chalcone **3** molecule per cell. The bonds around the piperidine N atom, C30–N31, N31–C36, N31–C32 are 1.4736 (15) 1.4705 (16) and 1.4740 (16) Å respectively which are slightly shorter than the normal C–N bond, 1.50

Table 2 Crystal data and structure refinement details for 2-Benzyloxynaphthylchalcone **3**

$C_{32}H_{31}NO_3C_2H_6O$	Mr = 523.64
F(000)= 560	
Triclinic, P-1 (no. 2)	Dx = 1.248 Mg m^{-3}
a = 10.6946 (5) Å	Mo Kα radiation, λ = 0.71073 Å
b = 11.7088 (5) Å	Cell parameters from 7929 reflections, θ = 3.3–32.4
c = 13.5975 (5) Å	θ = 3.3–32.4°
α = 96.356 (3)°	μ = 0.08 mm−1
β = 107.209 (4)°	T = 140 K
γ = 116.643 (5)°	Wedge, pale yellow
V = 1393.45 (12) Å3	0.43 × 0.28 × 0.23 mm
Z = 2	
Oxford Diffraction Xcalibur 3/Sapphire3 CCD diffractometer	6372 independent reflections
Radiation source: Enhance (Mo) X-ray Source	4826 reflections with I > 2σ(I) 'observed'
Graphite monochromator	Rint = 0.037
Detector resolution: 16.0050 pixels mm-1	θmax = 27.5°, θmin = 3.7°
R_1('observed' data) = 0.045	H atoms treated by a mixture of independent and constrained refinement
wR_2(all data) = 0.125	Weighting: $w = 1/[\sigma^2(Fo^2) + (0.059P)^2 + 0.130P]$ where $P = (Fo^2 + 2Fc^2)/3$
S = 1.09	(Δ/σ)max = 0.001
6372 reflections	Δρmax = 0.41 e $Å^{-3}$
360 parameters	Δρmin = −0.29 e $Å^{-3}$

Table 3 Selected geometric parameters (Å, °) of compound **3**

C2—O2	1.3627 (15)	C30—N31	1.4736 (15)
O2—C20	1.4366 (17)	N31—C36	1.4705 (16)
C13—O13	1.2293 (16)	N31—C32	1.4740 (16)
C17—O17	1.3574 (14)	O41—C42	1.429 (2)

O2—C2—C1	116.23 (11)	C30—N31—C32	111.00 (10)
O2—C2—C3	121.49 (12)	C2—O2—C20	120.63 (10)
O13—C13—C12	121.20 (11)	N31—C36—C35	110.18 (11)
O13—C13—C14	120.66 (11)	O41—C42—C43	112.99 (17)
O17—C17—C18	117.94 (12)	O17—C17—C16	121.79 (11)
O2—C20—C21	105.48 (11)		

Table 4 Hydrogen-bond geometry (Å, °) of compound **3**

D—H···A	D—H	H···A	D···A	D—H···A
C12—H12···O2	0.93	2.13	2.7297 (16)	121
C20—H20B···O41i	0.97	2.59	3.4797 (18)	153
O17—H17O···N31	0.93 (2)	1.73 (2)	2.6165 (16)	157.5 (16)
O41—H41O···O13	0.92 (3)	1.90 (3)	2.7980 (17)	168 (2)

Symmetry code: (i) x−1, y−1, z.

Å [35]. The molecule exhibits short intra- and inter-molecular interactions. An intramolecular hydrogen bond links the hydroxyl group of O(17) with the piperidine N(31) atom, and the solvent ethanol molecule forms a good hydrogen bond with the carbonyl O(13) atom, **Table 4** and **Fig. 3(a)**. The molecule comprises three planar aromatic ring groups and a chair-shaped piperidine ring. The hinge atoms between the planar groups are C(20) and C(12), with the piperidine group hinged at C(30). The naphthyl group lies parallel (at a distance of 3.476 Å), and related about a centre of symmetry, to a neighbouring group with extensive π…π interactions. The chain of C(11, 12, 13, 14, 19, 18, 17) and O(17) overlies a symmetry-related chain, also with close π…π interactions and at a distance of 3.375 Å. **Fig. 4(b). Fig. 3(b)** illustrates the molecular interactions in compound **3** by showing red, white and blue colors; the presence of red areas around some atoms indicates strong internal and external interactions.

'Fingerprint plots' from the Hirshfeld surface analysis, **Fig, 5**, show that H...H contacts have the highest number of interactions in compound **3**, (62.4%). The C···H/H···C contacts act as secondary interactions with sharp peaks (20.8%). H···N/N···H contacts show no role (0.0%), and O···H/H···O contacts account for 10.4% of interactions (di + de = 2.4 Å), (**Fig. 5**). Interestingly, C…C interactions for **3** account for 5.2% of contacts, indicating good π···π stacking.

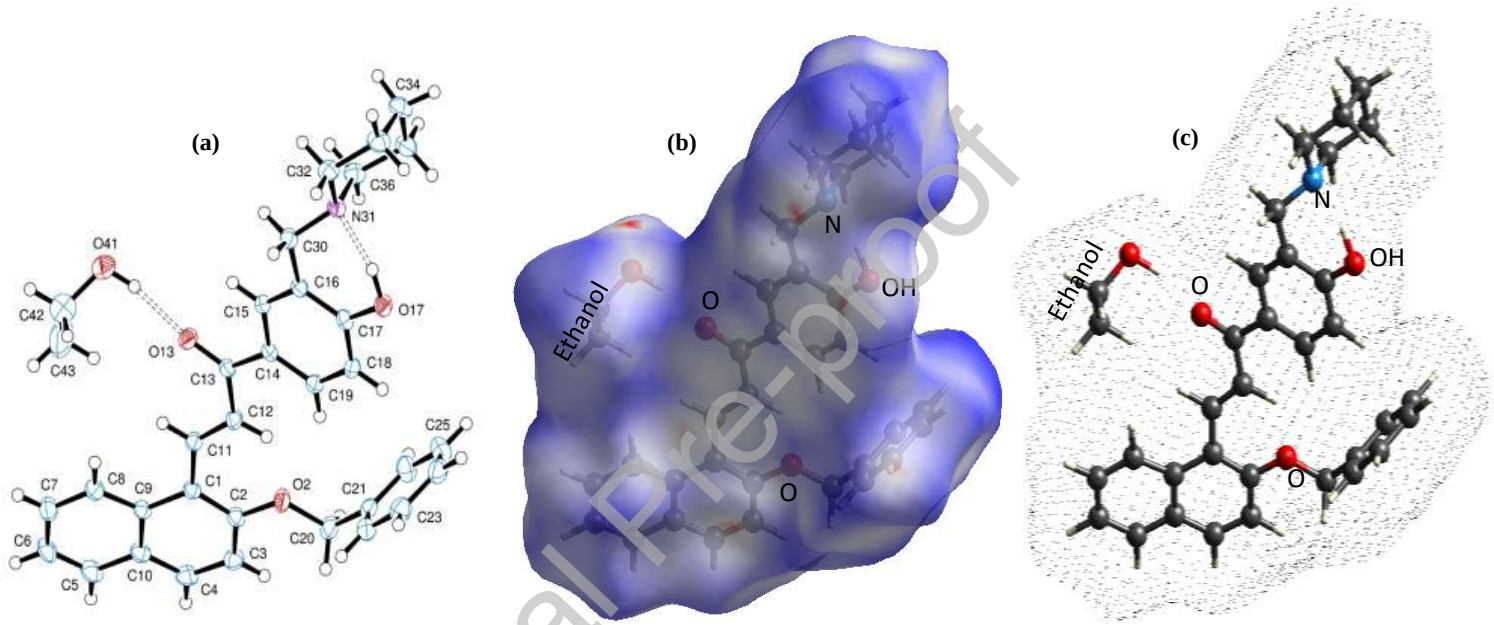

Fig. 3 (a) An ORTEP diagram of **3** showing the atom-labelling scheme. Thermal ellipsoids are shown at 50% probability, (b) Hirshfeld surfaces views of the molecule **3** mapped over d_{norm} with enabled surface transparency. The red and blue regions represent negative and positive electrostatic potentials, respectively, (c) Mesh diagram of **3** showing the molecule with the extent of the electron density around it.

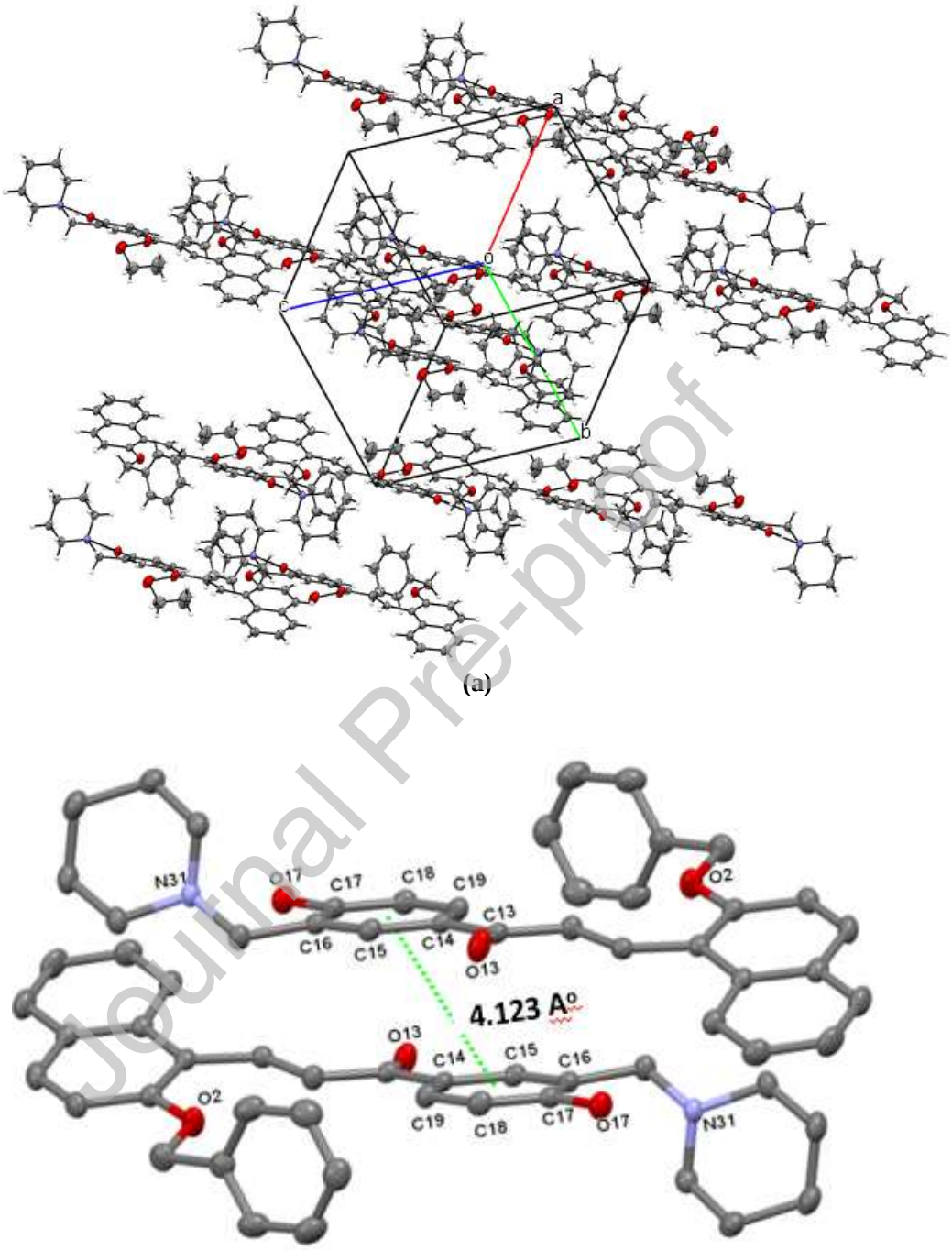

Fig. 4 (a) A projected view of the molecular packing of **3, (b)** A pair of overlaying molecules of **3** showing the distance between calculated centroids. The distance between the overlapping rings is *ca* 3.42 Å. This view was drawn using Mercury [36]. Hydrogen atoms are omitted for clarity and were not included in the distance calculation.

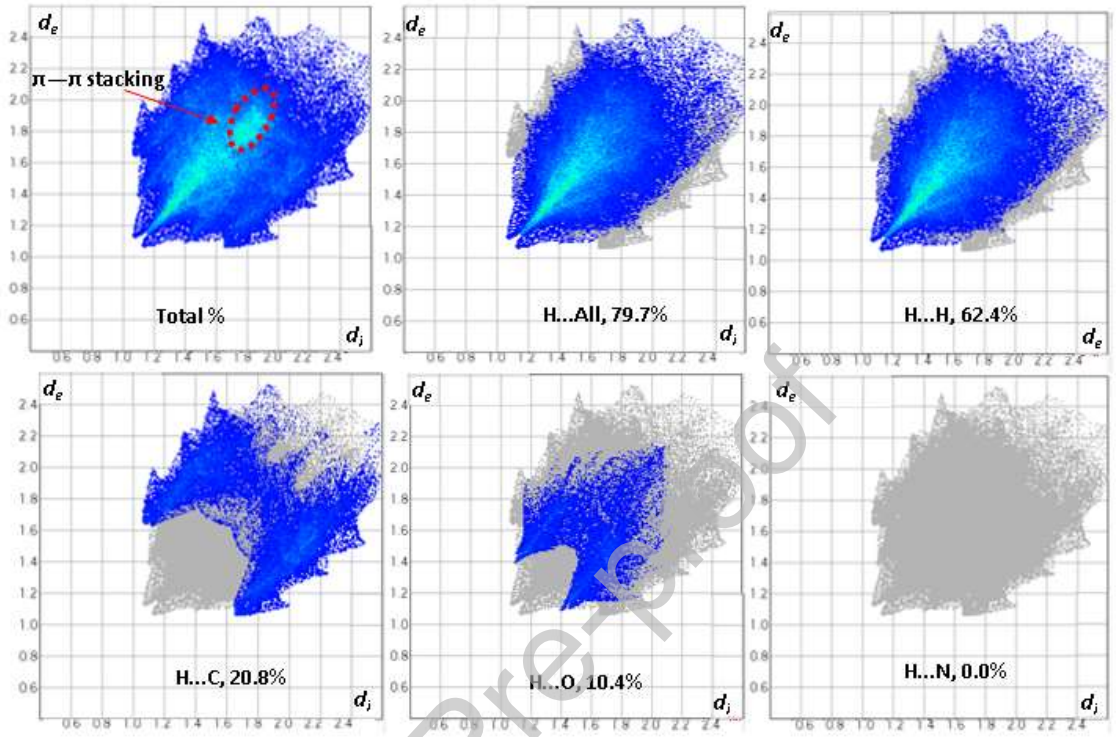

Fig. 5 Two-dimensional fingerprint plots for compound **3**: for Total, H···All, H···H, H···C, H···O and H···N interactions. The outline of the full fingerprint is shown in gray. di is the closest internal distance from a given point on the Hirshfeld surface and de is the closest external distance.

3.3 Metal-chelating properties

Considering the implications of metals in AD pathogenesis, the chelating ability of chalcone **3** toward biometals such as Cu^{2+}, Fe^{2+}, Al^{3+}, and Zn^{2+}, was evaluated using ultraviolet-visible (UV–Vis) spectrometry. The metal complexation capacity of chalcone **3** was investigated *in situ* using UV−Vis absorption. Interestingly, the maximum absorption at 338 nm was shifted to 307 nm after the addition of $FeCl_2$, which indicated the possible formation of a **3**-Fe^{2+} complex. The difference in the UV−Vis absorption peaks (31 nm) between the free ligand and the Fe(II) complex is probably due to changes in the molecular/electronic conformation effect caused by complexation, **Figs. 6 and 8**

[37]. The addition of $AlCl_3$ and $CuCl_2$ exhibited marginal blue shift of the maximum absorption from 338 to 329 nm. However, no significant change was observed with the addition of $ZnCl_2$.

To consider the stoichiometry of the resulting complex **3**-Fe^{2+} using the molar ratio method, chalcone **3** in a fixed concentration (60 μM) was mixed with increasing concentrations of $FeCl_2$ (6-100 μM). The absorbance of the resulting complex of $FeCl_2$ and **3** was recorded using a UV-Vis spectrometer at 307 nm. As displayed in **Fig 7**, the absorbance increased linearly at first, before plateauing when the mole fraction of Fe^{2+} to **3** was about 0.9, indicating a 1:1 stoichiometry for complex **3**-Fe^{2+}.

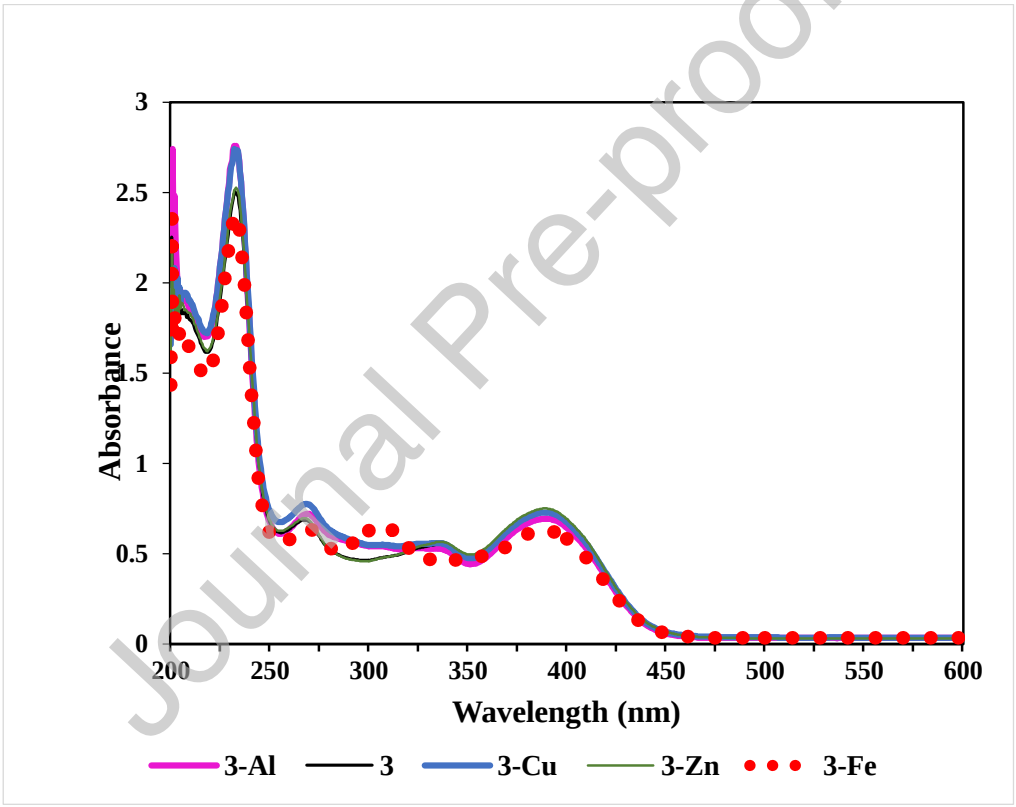

Fig. 6 UV−Vis spectra of chalcone **3** in methanol (60 μM) alone and titrated with $CuCl_2$, $FeCl_2$, $ZnCl_2$ or $AlCl_3$ (60 μM in methanol)

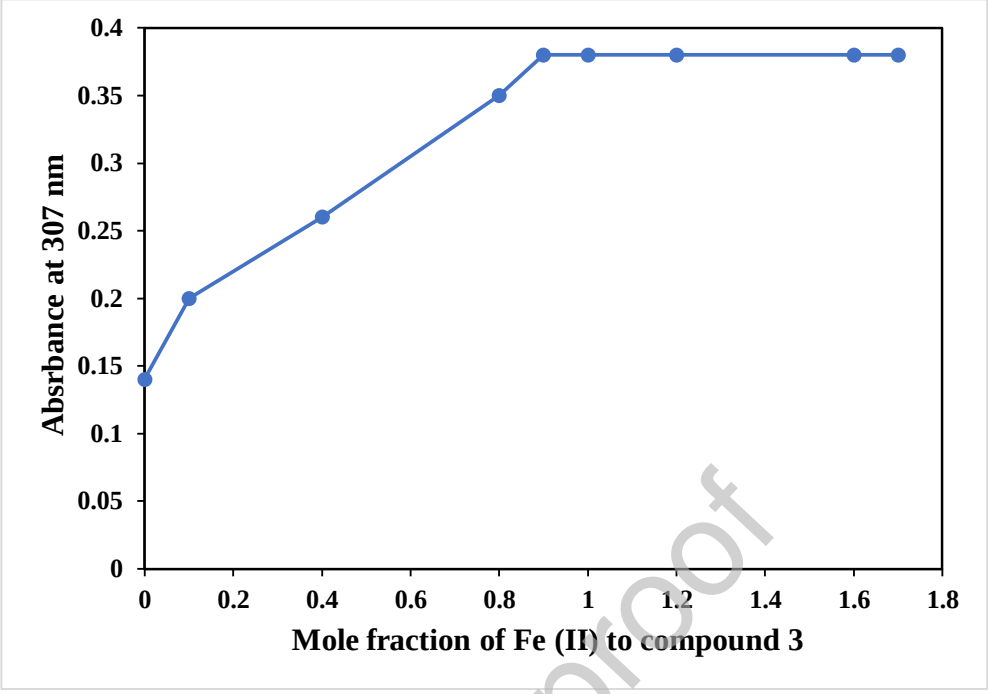

Fig. 7 The stoichiometry of complex **3**-Fe^{2+} via the molar ratio method

To highlight the metal chelating sites a deuterium methanolic solution of chalcone **3** (19 µM) was titrated *in situ* with increasing equivalents of $FeCl_2$ solution (19 µM). The progress of the complexation was monitored using ^1H NMR spectroscopy as presented in **Fig. 8**. The spectra indicated that the signals of the piperidine protons have been split to five different signals due to the coordination of Fe^{+2} with the nitrogen atom; compared to the crystal structure ^1H NMR spectrum, which showed three broad singlet signals attributed to three sets of equivalent CH_2 groups of the piperidine moiety, this suggests that the chalcone conformation was changed upon complexation. Moreover, the methylene protons (H_b) have been shifted upfield upon complexation. Similarly, the benzyloxy protons have been shifted upfield which indicated coordination via its oxygen. The structure involved the ferrous(II) ion being coordinated through the lone pair electrons of both nitrogen and oxygen atoms, correlated to Mannich base and benzyloxy moieties respectively, and forming, probably, an octahedral structure, the common geometric structure for Fe(II) in the presence of water/methanol molecules in solution [38]. Because it was not possible to obtain a suitable single crystal for X-ray study, the geometric structure for Fe(II) may not be fully confirmed. The IR spectra have proven to

be a suitable tool to provide enough information for us to describe the way of bonding of the ligands. Therefore, a detailed elucidation of IR spectra of the chalcone ligand and the effect of binding of iron(II) on the vibration frequencies of the chalcone ligand are highlighted to conclude that the coordination mode involves chelation. The IR spectrum of the precipitated complex (**3**-Fe^{2+}) confirmed the coordination sites due to the presence of a broad absorption band at 3432 cm^{-1} for the hydroxyl group and a very weak stretching vibration at 2946 cm^{-1} for the aliphatic C-H. Additionally, it showed an absorption frequency at 1604 cm^{-1} implying the presence of a conjugated carbonyl group adjacent to the C=C group, with characteristic olefinic peak at 1641 cm^{-1} (**Fig S4**).

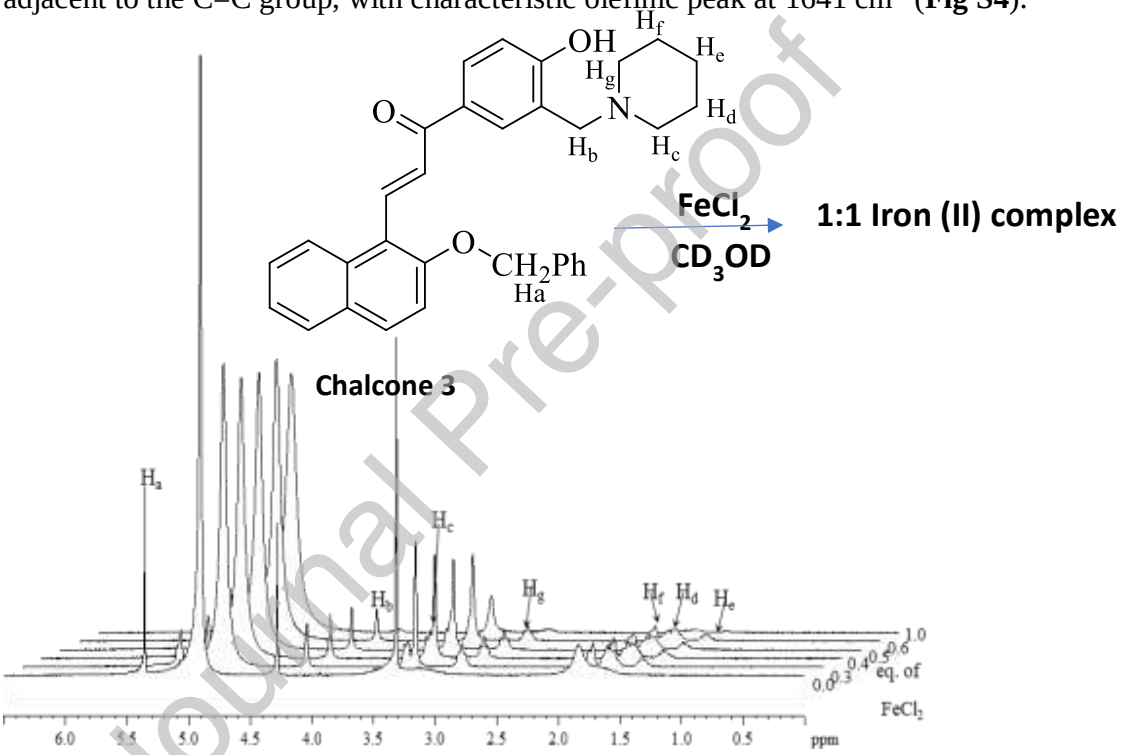

Fig. 8 ^{1}H-NMR titration of compound **3** with $FeCl_2$ in CD_3OD. Spectra 2-6 recorded upon the addition of increasing eq. of $FeCl_2$

*3.4 In vitro bioactivity evaluations of chalcone **3***

The novel chalcone **3** exhibited potent inhibitory activity against *Electric eel* AChE with IC_{50} 1.0 nM showing better inhibition than donepezil (IC_{50}. 33.4 nM). Furthermore, it showed comparable scavenging inhibitory activity towards DPPH comparable to that of ascorbic acid with a 3-fold difference, as displayed in **Table 5**.

Table 5 Cholinesterase and DPPH activities of chalcone **3**

Compound	AChE IC_{50} (nM) ± SD	DPPH Radical IC_{50} µg/ml
3	1.0± 0.003	55.52 ± 1.1
Donepezil	33.4 ± 0.002	-
AA	-	17.96 ± 0.4

IC_{50} ±SD: Inhibitor concentration (mean ± S.D. of three experiments) needed for 50% inhibition of the enzyme; AA (Ascorbic acid)

*3.5 Binding prediction of chalcone **3** using molecular docking*

Docking analysis was carried out using the elucidated crystal structure data of chalcone **3** to screen its binding affinity on the *Torpedo california* acetylcholinesterase (TcAChE) (PDB 1EVE). Chalcone **3** displayed tight binding against the TcAChE enzyme with low binding energy -13.29 kcal/mol in comparison to donepezil (-10.52 kcal/mol). Superimposition of **3** (yellow stick) and donepezil (grey stick) as shown in **Fig. 9** demonstrates the benzylic moiety in ring B is directed towards the peripheral anionic site (PAS), while the three planar aromatic rings of chalcone **3** turned the piperidine ring towards the catalytic anionic site (CAS) similar to donepezil. We note that the molecular structure of **3** has changed drastically after binding with the protein when compared to the free molecule. Comparison of the interactions of chalcone **3** and donepezil within the active site of AChE revealed that there is considerable flexibility of the chalcone **3** molecule that facilitates the interaction between piperidine and the binding site for the quaternary nitrogen of AChE, TRP84 via π-alkyl interactions with distances of 5.30 and 5.01 Å in line with donepezil (**Fig. 9**). TRP84 was considered the principal component of the anionic site [39]. However, two hydrogen bonds were found between the hydroxyl group at ring A of **3** and residues GLY118, and GLU199 at the oxyanion site with distances 2.87 and 2.18 Å respectively **Fig**. **10**(a). Moreover, a hydrogen bond was found between the hydroxyl group of TYR121 at the PAS site and benzyloxy group at ring B with distance 2.65 Å. Furthermore, hydrophobic interaction with the PAS was observed between the benzyl moiety of chalcone **3** and the residue ASP70. This residue is a vital component of the PAS site as several studies have reported its role as a trap for charged

substrate, thus contributing to catalytic efficiency. Similar transient binding also occurs with cationic organophosphates [40,41]. It is also worth noting that at the bottom of the gorge, a CH···π T-shaped hydrophobic interaction was observed between ring A of chalcone **3** and the phenyl moiety of HIS440, a residue of the catalytic triad in the active site of AChE [42]. These interactions were not observed in donepezil and might contribute to the affinity to the enzyme hence improving the inhibition effect of chalcone **3**. Overlay of the crystallographic structure (magenta) and the docked (green) conformations of chalcone **3** suggests that the presence of methylene groups might be responsible for the chalcone structural flexibility as presented in **Fig. 11.**

Therefore, we propose that the novel chalcone **3** shows potent *in vitro* inhibitory activity towards AChE when compared with donepezil.

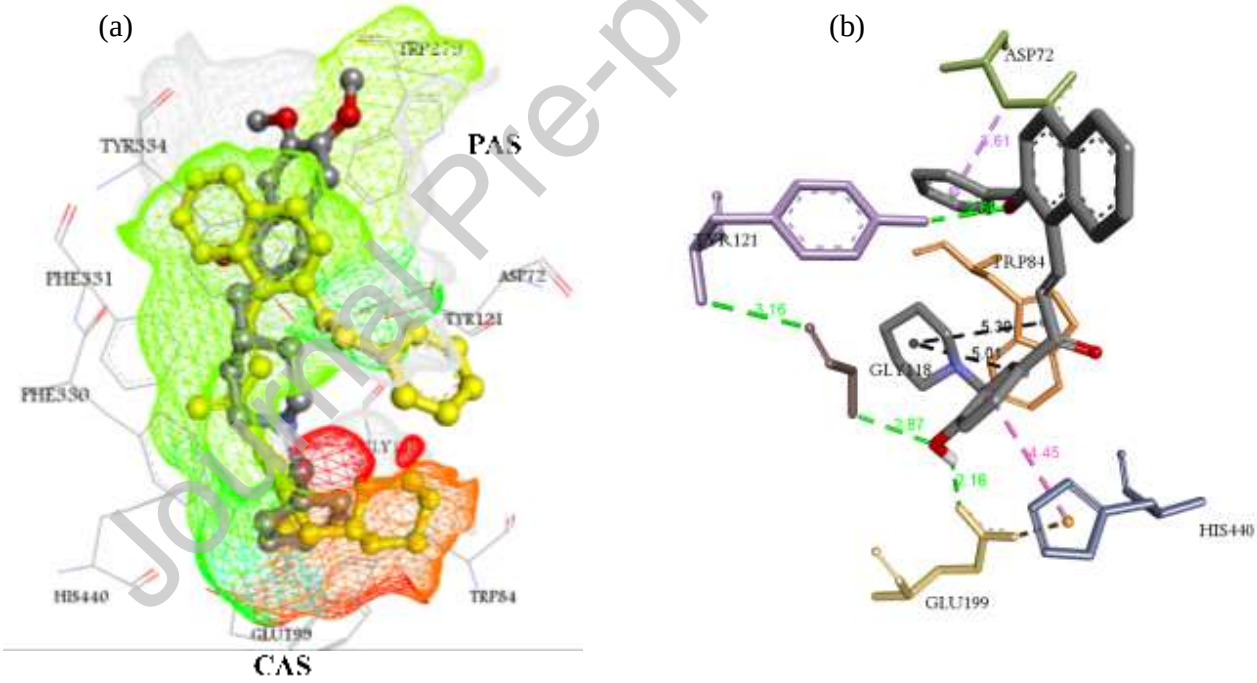

Fig. 9 Docking model of TcAChE-**3** complex showing superimposition of the ligand **3** (yellow stick) with donepezil (grey stick) in the active site of 1EVE (**a**). The interacting mode of chalcone **3** in the active gorge of TcAChE, (**b**)

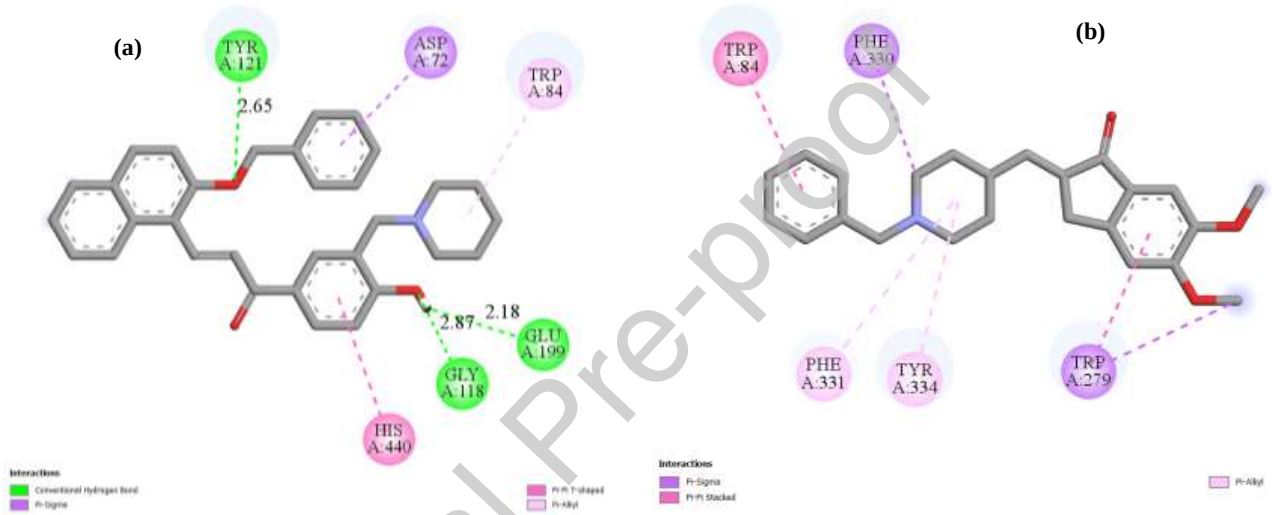

Fig. 10 2D representations of interactions in the TcAChE- **3** complex (**a**) and in the TcAChE-donepezil complex(**b**)

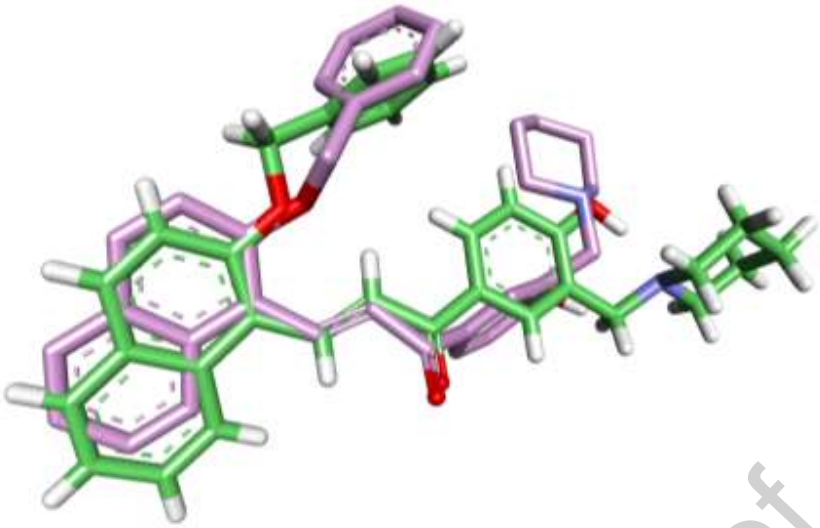

Fig. 11 Overlay of crystallographic (magenta) and docked (green) conformations of chalcone **3**

4. Conclusion

Interesting HS analysis was accomplished for the 2-benzyloxynaphthalene aminoalkylated chalcone **3**. The *in vitro* analysis of chalcone **3** showed potent inhibitory activity against AChE with moderate scavenging ability toward DPPH. Moreover, the chalcone **3** was able to coordinate with the biometal $FeCl_2$ in a stoichiometry ratio 1:1 to form the complex **3**-Fe^{2+} based on the UV−Vis and the NMR analysis. Molecular docking analysis was used to further explore the binding mode of **3** with AChE and to investigate the efficacy of introducing Mannich base and benzyl moieties into a naphthalene-based chalcone. The molecular modelling proves the potential inhibition activity of **3** against AChE due to the presence of three hydrogen bonds with the PAS and oxyanion site of 1EVE. Also, different critical hydrophobic interactions were observed with the CAS amino acids and HIS440, a crucial residue of the catalytic triad. Taken together, these preliminary findings present a starting point for development of multifunctional agents for the treatment of AD in future.

5. Supplementary data:

CCDC 1973469 contains the crystallographic data for compound **3**. These data can be obtained free of charge via www.ccdc.cam.ac.uk/data_ request/cif or from the Cambridge

Crystallographic Data Centre, 12 Union Road, Cambridge CB2 1EZ, UK; fax: (þ44) 1223 336 033; or e-mail: deposit@ccdc.cam.ac.u.k.

6. Acknowledgment: The authors are grateful for the financial support from Taibah University and the technical assistance from UTM (4F830). M. A. Said is thankful to Alexander von Humboldt Stiftung, Germany, for the opportunities provided.

Credit Author Statement

Author Contributions:

Conceptualization, N.B, A.A.A. S.Y.A. and G. A.

Methodology and Docking, G.A.

All authors, Writing-Review & Editing

D.L. and M.A.S; X-ray work

M.A.; HSA work.

CONFLICT OF INTEREST

NO CONFLICT OF INTEREST

7. References

[1] S.L. Gaonkar, U.N. Vignesh, Synthesis and pharmacological properties of chalcones: a review, Res. Chem. Intermed. 43 (2017) 6043–6077. doi:10.1007/s11164-017-2977-5.

[2] P. Singh, A. Anand, V. Kumar, Recent developments in biological activities of chalcones: A mini review, Eur. J. Med. Chem. 85 (2014) 758–777. doi:10.1016/j.ejmech.2014.08.033.

[3] Z. Ates-Alagoz, T. Coban, E. Buyukbingol, Synthesis and Antioxidant Activity of New Tetrahydro-Naphthalene-Indole Derivatives as Retinoid and Melatonin Analogs, Arch. Pharm. (Weinheim). 339 (2006) 193–200. doi:10.1002/ardp.200500177.

[4] S. Banerjee, E.B. Veale, C.M. Phelan, S.A. Murphy, G.M. Tocci, L.J. Gillespie, D.O.

Frimannsson, J.M. Kelly, T. Gunnlaugsson, Recent advances in the development of 1,8-naphthalimide based DNA targeting binders, anticancer and fluorescent cellular imaging agents, Chem. Soc. Rev. 42 (2013) 1601–1618. doi:10.1039/c2cs35467e.

[5] K. Venkatesan, V.S. V. Satyanarayana, A. Sivakumar, Ultrasonic Assisted Synthesis of Naphthalene Substituted Schiff Base Derivatives and Their Antioxidant Activity Studies, J. Chinese Chem. Soc. 58 (2011) 583–589. doi:10.1002/jccs.201190091.

[6] A. Rauf, H. Subhan, R. Abbasi, B. Adhikari, A.H. Shah, U.A. Rana, Q. Abbas, I.Z. Qureshi, H. Hussain, K. Mazhar, A. Badshah, H.B. Kraatz, A. Shah, Biological activity, pH dependent redox behavior and UV-Vis spectroscopic studies of naphthalene derivatives, J. Photochem. Photobiol. B Biol. 140 (2014) 173–181. doi:10.1016/j.jphotobiol.2014.07.010.

[7] J.P. Jasinski, R.J. Butcher, A.N. Mayekar, H.S. Yathirajan, B. Narayana, Structures of three chalcones derived from 6-methoxy-2-naphthaldehyde, J. Chem. Crystallogr. 39 (2009) 157–162. doi:10.1007/s10870-008-9446-3.

[8] K. Thanigaimani, S. Arshad, N.C. Khalib, I.A. Razak, C. Arunagiri, A. Subashini, S.F. Sulaiman, N.S. Hashim, K.L. Ooi, A new chalcone structure of (E)-1-(4-Bromophenyl)-3-(napthalen-2-yl)prop-2-en-1-one: Synthesis, structural characterizations, quantum chemical investigations and biological evaluations, Spectrochim. Acta - Part A Mol. Biomol. Spectrosc. 149 (2015) 90–102. doi:10.1016/j.saa.2015.04.028.

[9] World Health Organisation, Dementia Fact Sheet No.362, World Heal. Organ. Geneva, Switzerland,. 2013 (2015).

[10] M. Weinstock, Selectivity of Cholinesterase Inhibition, CNS Drugs. 12 (1999) 307–323. doi:10.2165/00023210-199912040-00005.

[11] J.K. Dhanjal, S. Sharma, A. Grover, A. Das, Use of ligand-based pharmacophore modeling and docking approach to find novel acetylcholinesterase inhibitors for treating Alzheimer's, Biomed. Pharmacother. 71 (2015) 146–152. doi:10.1016/j.biopha.2015.02.010.

[12] L. Wang, Y. Wang, Y. Tian, J. Shang, X. Sun, H. Chen, H. Wang, W. Tan, Design, synthesis, biological evaluation, and molecular modeling studies of chalcone-rivastigmine hybrids as cholinesterase inhibitors, Bioorganic Med. Chem. 25 (2017) 360–371. doi:10.1016/j.bmc.2016.11.002.

[13] X. Zhang, Q. Song, Z. Cao, Y. Li, C. Tian, Z. Yang, H. Zhang, Y. Deng, Design, synthesis and evaluation of chalcone Mannich base derivatives as multifunctional agents for the potential treatment of Alzheimer's disease, Bioorg. Chem. 87 (2019) 395–408. doi:10.1016/j.bioorg.2019.03.043.

[14] C. Tian, X. Qiang, Q. Song, Z. Cao, C. Ye, Y. He, Y. Deng, L. Zhang, Flurbiprofen-chalcone hybrid Mannich base derivatives as balanced multifunctional agents against Alzheimer's disease: Design, synthesis and biological evaluation, Bioorg. Chem. 94 (2020) 103477. doi:10.1016/j.bioorg.2019.103477.

[15] A.I. Bush, R.E. Tanzi, Therapeutics for Alzheimer's Disease Based on the Metal Hypothesis, Neurotherapeutics. 5 (2008) 421–432. doi:10.1016/j.nurt.2008.05.001.

[16] X. Wang, X. Wang, Z. Guo, Metal-involved theranostics: An emerging strategy for fighting Alzheimer's disease, Coord. Chem. Rev. 362 (2018) 72–84.

doi:10.1016/j.ccr.2018.03.010.

[17] A. Rauk, The chemistry of Alzheimer's disease, Chem. Soc. Rev. 38 (2009) 2698. doi:10.1039/b807980n.

[18] K.P. Kepp, Bioinorganic chemistry of Alzheimer's disease, Chem. Rev. 112 (2012) 5193–5239. doi:10.1021/cr300009x.

[19] J.H. Viles, Metal ions and amyloid fiber formation in neurodegenerative diseases. Copper, zinc and iron in Alzheimer's, Parkinson's and prion diseases, Coord. Chem. Rev. 256 (2012) 2271–2284. doi:10.1016/j.ccr.2012.05.003.

[20] M. Kawahara, M. Kato-Negishi, Link between Aluminum and the Pathogenesis of Alzheimer's Disease: The Integration of the Aluminum and Amyloid Cascade Hypotheses., Int. J. Alzheimers. Dis. 2011 (2011) 276393. doi:10.4061/2011/276393.

[21] C.X. Xie, M.P. Mattson, M.A. Lovell, R.A. Yokel, Intraneuronal aluminum potentiates iron-induced oxidative stress in cultured rat hippocampal neurons, Brain Res. 743 (1996) 271–277. doi:10.1016/S0006-8993(96)01055-4.

[22] G. Aljohani, D. Lentz, M.A. Said, S.Y. Alraqa, A.A. Ali, N. Basar, Crystal Structure of 2-(prop-2-yn-1-yloxy)-1-naphthaldehyde, C14H10O2, Zeitschrift Für Krist. - New Cryst. Struct. 234 (2019) 977–978. doi:10.1515/ncrs-2019-0195.

[23] G. Aljohani, M.A. Said, D. Lentz, N. Basar, A. Albar, S.Y. Alraqa, A. Al-Sheikh Ali, Microwave-Assisted Synthesis of Mono- and Disubstituted 4-hydroxyacetophenone Derivatives via Mannich Reaction: Synthesis, XRD and HS-Analysis, Molecules. 24 (2019) 590. doi:10.3390/molecules24030590.

[24] V. Calvino, M. Picallo, A.J. López-Peinado, R.M. Martín-Aranda, C.J. Durán-Valle, Ultrasound accelerated Claisen-Schmidt condensation: A green route to chalcones, Appl. Surf. Sci. 252 (2006) 6071–6074. doi:10.1016/j.apsusc.2005.11.006.

[25] M.J. Climent, A. Corma, S. Iborra, J. Primo, Base catalysis for fine chemicals production: Claisen-schmidt condensation on zeolites and hydrotalcites for the production of chalcones and flavanones of pharmaceutical interest, J. Catal. 151 (1995) 60–66. doi:10.1006/jcat.1995.1008.

[26] M.R. Jayapal, K. Sreenivasa Prasad, N.Y. Sreedhar, Synthesis and characterization of 2,4-dihydroxy substituted chalcones using aldol condensation by SOCl 2 / EtOH, J. Chem. Pharm. Res. 2 (2010) 127–132. www.jocpr.com.

[27] O.D. Rigaku, CrysAlis PRO Software System, Rigaku Oxford Diffr. Ltd, Yarnton, Oxfordshire, Engl. (2018).

[28] G.M. Sheldrick, (a) *SHELXT* – Integrated space-group and crystal-structure determination. Acta Crystallogr. Sect. A Foundations and Advances 71, (2015) 3-8. doi.org/10.1107/S2053273314026370; (b) Crystal structure refinement with SHELXL, Acta Crystallogr. Sect. C Struct. Chem. 71 (2015) 3–8. doi:10.1107/S2053229614024218.

[29] L.J. Farrugia, WinGX and ORTEP for Windows: An update, J. Appl. Crystallogr. 45 (2012) 849–854. doi:10.1107/S0021889812029111.

[30] M.J. Turner, J.J. McKinnon, S.K. Wolff, D.J. Grimwood, P.R. Spackman, D. Jayatilaka, M.A. Spackman, CrystalExplorer. Version 17. University of Western Australia, (2017).

[31] I. Hamad, H. AbdElgawad, S. Al Jaouni, G. Zinta, H. Asard, S. Hassan, M. Hegab, N. Hagagy, S. Selim, Metabolic Analysis of Various Date Palm Fruit (Phoenix dactylifera L.) Cultivars from Saudi Arabia to Assess Their Nutritional Quality, Molecules. 20 (2015) 13620–13641. doi:10.3390/molecules200813620.

[32] Y.-H. Koay, A. Basiri, V. Murugaiyah, K.-L. Chan, Isocorilagin, a Cholinesterase Inhibitor from Phyllanthus niruri, Nat. Prod. Commun. 9 (2014) 515–517. doi:10.1177/1934578X1400900423.

[33] G.M. Morris, H. Ruth, W. Lindstrom, M.F. Sanner, R.K. Belew, D.S. Goodsell, A.J. Olson, AutoDock4 and AutoDockTools4: Automated docking with selective receptor flexibility, J. Comput. Chem. 30 (2009) 2785–2791. doi:10.1002/jcc.21256.

[34] Dassault Systèmes BIOVIA, Discovery Studio Modeling Environment, Release 2017, San Diego: Dassault Systèmes, (2016).

[35] F.H. Allen, O. Kennard, D.G. Watson, L. Brammer, A.G. Orpen, R. Taylor, Tables of bond lengths determined by X-ray and neutron diffraction. Part 1. Bond lengths in organic compounds, J. Chem. Soc. Perkin Trans. 2. 0 (1987) S1. doi:10.1039/p298700000s1.

[36] C.F. Macrae, P.R. Edgington, P. McCabe, E. Pidcock, G.P. Shields, R. Taylor, M. Towler, J. Van De Streek, Mercury: Visualization and analysis of crystal structures, J. Appl. Crystallogr. 39 (2006) 453–457. doi:10.1107/S002188980600731X.

[37] L.H. Abdel-Rahman, R.M. El-Khatib, L.A.E. Nassr, A.M. Abu-Dief, Synthesis, physicochemical studies, embryos toxicity and DNA interaction of some new Iron(II) Schiff base amino acid complexes, J. Mol. Struct. 1040 (2013) 9–18. doi:10.1016/j.molstruc.2013.02.023.

[38] L.H. Abdel-Rahman, R.M. El-Khatib, L.A.E. Nassr, A.M. Abu-Dief, M. Ismael, A.A. Seleem, Metal based pharmacologically active agents: Synthesis, structural characterization, molecular modeling, CT-DNA binding studies and in vitro antimicrobial screening of iron(II) bromosalicylidene amino acid chelates, Spectrochim. Acta - Part A Mol. Biomol. Spectrosc. 117 (2014) 366–378. doi:10.1016/j.saa.2013.07.056.

[39] G. Kryger, I. Silman, J.L. Sussman, Structure of acetylcholinesterase complexed with E2020 (Aricept®): Implications for the design of new anti-Alzheimer drugs, Structure. 7 (1999) 297–307. doi:10.1016/S0969-2126(99)80040-9.

[40] G. Johnson, S. Moore, The Peripheral Anionic Site of Acetylcholinesterase: Structure, Functions and Potential Role in Rational Drug Design, Curr. Pharm. Des. 12 (2005) 217–225. doi:10.2174/138161206775193127.

[41] N.A. Hosea, Z. Radić, I. Tsigelny, H.A. Berman, D.M. Quinn, P. Taylor, Aspartate 74 as a Primary Determinant in Acetylcholinesterase Governing Specificity to Cationic Organophosphonates, Biochemistry. 35 (1996) 10995–11004. doi:10.1021/bi9611220.

[42] J.L. Sussman, M. Harel, F. Frolow, C. Oefner, A. Goldman, L. Toker, I. Silman, Atomic structure of acetylcholinesterase from Torpedo californica: A prototypic acetylcholine-binding protein, Science (80-.). 253 (1991) 872–879. doi:10.1126/science.1678899.

GRAPHICAL ABSTRACT